PHYSICS BASED APPROACHES FOR ACTIVE ROTOR CONTROL TECHNOLOGY

Lakshmi N. Sankar and JVR Prasad
School of Aerospace Engineering, Georgia Institute of Technology, Atlanta, GA, USA

Chengjian He
Advanced Rotorcraft Technology, Inc. Sunnyvale, CA, USA

Abstract

A methodology for physics based reduced order modeling of next generation OBC concepts suitable for fast and real time simulations has been integrated with a computationally efficient framework for extraction of time-invariant linearized models suitable for handling qualities assessment and integrated flight and rotor control design and analyses. The accuracy of the developed reduced-order models has been evaluated through comparisons with high fidelity CFD predictions and available test data. The reduced order models have been integrated into the modular architecture of FLIGHTLAB simulation model for fast and real time demonstrations. New algorithms have been developed by exploiting the harmonic domain representation of rotor states for extraction of LTI models of coupled body-rotor dynamics suitable for various control design applications with IBC and OBC concepts and for handling qualities assessment. The extracted LTI models have been validated through comparisons with the nonlinear model predictions in time and frequency domains.

1. INTRODUCTION

Current flight controller designs for helicopters represent a difficult trade-off between controller bandwidth and its impact on rotor stability, and rotor vibratory loads. Traditional swashplate controls in terms of collective, longitudinal cyclic and lateral cyclic limit the number of controls available to the control designer in addressing flight and rotor control issues. For example, a four-bladed rotor using IBC has four independent controls available. However, the use of swashplate for control inputs restricts the number of independent controls to only three, limiting the design space available to the control system designer.

Individual Blade Control (IBC) and On-Blade Control (OBC) concepts offer tremendous potential for expanding the available control design space, and allow tailoring the control input signals for desired blade responses to address flight and rotor control issues in a unified framework. IBC and OBC concepts offer the potential to develop innovative controllers for mitigation of compressibility effects on advancing blades and reverse flow effects on retreating blades for improved rotor performance, control of an individual blade that may be off-track, mitigation of transient effects associated with rotor speed variations, mitigation of undesirable coupling between body and rotor in large size helicopters due to increased rotor blade flexibility, reduction of maneuver blade and rotor loads, reduction of vibratory hub loads, and the reduction of blade-vortex interaction noise, while ensuring good flying qualities as specified in the Aeronautical Design Standard (ADS-33). While higher flight control bandwidth can be achieved through innovative integrated flight and rotor control designs, the implications of such higher bandwidth control arising out of IBC and OBC concepts on handling qualities and vehicle-pilot-biodynamic coupling need to be carefully assessed before they can be fully realized.

Higher harmonic control of swashplate,[1,2] individual blade control[3-6] and on-blade control[7-9] applications both in wind tunnel and flight tests have been documented extensively in the literature. Expansion of the control space through IBC/OBC has enabled researchers to show possibilities of extensive improvements for reduced power.[1,3,7] vibration[1,3,7], and noise.[3,4,7] Along with these primary improvements, even additional capabilities emerged such as gust alleviation[9], correction of the blade tracking problems due to dissimilarity between blades, and higher redundancy for safety and reliability[10] of a modern helicopter. These studies have focused on the rotor control applications alone without assessing their effect on handling

qualities.

Higher harmonic control using on-blade control will require high fidelity aerodynamic analysis which includes changes in angle of attack and on-blade control deflections as well as deflection rates. This has been achieved in the literature by coupling Computational Fluid Dynamics (CFD) methods with comprehensive flight dynamic analyses codes.[11] Unfortunately, the state-of-the art CFD plus Computational Structural Dynamics (CSD) analyses tools for assessing the implications of IBC and OBC concepts are computationally expensive and are not suitable for controller synthesis, analysis, simulations and handling qualities assessment needed in the design cycle.

2. Research Goals and Approach

In order to address the needs discussed above, the present study is aimed at the development of a methodology for the generation of physics based reduced order models of next generation OBC concepts suitable for fast and real time simulations.

The following approach has been used. A data base of the impact of various OBC concepts on rotor aerodynamics using high fidelity CFD models is first generated. Using the generated data base and available test data, physics based reduced order models of next generation OBC concepts suitable for fast and real time simulations have been developed. The prediction accuracy of the reduced order models has been evaluated through comparisons with comprehensive CFD predictions and available test data. Finally, OBC controllers are developed using an optimization technique, where the hub vibratory loads minimized through a judicious selection of actuator locations, actuator size, and actuator motion amplitude.

3. Sample On-Board Control Concepts

A number of OBC concepts have been studied by the present investigators. For brevity, only a few of these are shown in this work. These aerodynamic calculations were done using Reynolds-Averaged Navier-Stokes (RANS) solvers. Most of the studies employed 2-D and 3-D Navier-Stokes analyses developed at Georgia Tech. Some of the analyses used the NASA OVERFLOW 2 software. In all applications, parametric studies were done to select a suitable computational grid, a suitable algorithm with acceptable spatial accuracy, and a suitable turbulence model capable of satisfactorily resolving the features of the separated flow.

3.1 Deformable Leading Edge (DDLE) Concept for Alleviating Dynamic Stall

It is well known that an active or passive leading edge droop can alter the dynamic stall characteristics of airfoils and rotors substantially. Calculations were done for a DDLE airfoil using the Georgia Tech in-house solver, DSS2. In this approach, the airfoil shape is gradually changed, and the leading edge radius is increased as the airfoil pitches up. Airfoils with large leading edge radii tend to have mild adverse pressure gradients, because the peak local velocities are lower than that for a conventional airfoil. As the airfoil pitches down, and there is no danger of stall, the airfoil returns to its original shape.

The reduced frequency $k= \omega b/V$ is 0.05, where b is the airfoil semi-chord, and V the free-stream velocity. The Free-stream Mach number is 0.3. The mean angle of attack is 10 degrees, and the amplitude of oscillation is 10 degrees as well. These parameters correspond to the experiment described in a paper by Chandrasekhara et al.[15]

Preliminary numerical results for this concept have been presented by the present researchers.[16] Figure 1 shows how the leading edge shape varies with time. Figure 2 shows the dynamic stall hysteresis loops for the DDLE airfoil and the baseline NACA 0012 airfoil. It is clearly seen that the DDLE has a smooth rise and drop in the lift coefficient as the airfoil pitches up and down. The variations in pitching moment are mild indicating that the resulting pitch link loads is also small.

3.2 Drooped leading Edge Concept

Calculations have also been done for static drooped leading edge concepts to assess their influence on dynamic stall characteristics. A NACA 0012, an Ames-01 airfoil, a VR-7 airfoil, and an SC 1095 airfoil with a fixed leading edge droop have been studied. Figures 3 shows the configurations with and without droop. Figure 4 shows the surface pressure contours at selected instances in time for representative airfoils. It is

clearly seen that the leading edge droop, even in a static manner, substantially alters the leading edge vortex formation, and mitigates the dynamic stall events.

The effect of the drooped leading edge airfoil on peak lift, drag, and moment are summarized in Table 1.

4. Reduced Order Models

The development of a reduced order model (ROM) is aimed at capturing the essential physics of the impact of selected OBC concepts on blade aerodynamics. A Neural Network (NNET) technique has been adopted for the ROM derivation. Neural Networks, or artificial neural networks to be more precise, represent a technique that is rooted in many disciplines: neuroscience, mathematics, physics, computer science, and engineering.[17]

Neural networks find widespread applications in such diverse fields as modeling and data processing. A neural network, made up of an interconnection of nonlinear neurons, is itself nonlinear. Nonlinearity is a highly important property, particularly for mapping rotorcraft aerodynamics, which are inherently nonlinear.

For OBC applications, the reduced order airloads model is formulated as a superposition of a baseline airloads model and the incremental difference between the baseline and the CFD simulation. The baseline airloads model can be a conventional engineering model without the effects of OBC. The incremental difference or the delta airloads is derived by subtracting the CFD results from the baseline airloads model and formulated as a NNET presentation. The following summarizes the formulation of the ROM.

In the present implementation, a quasi-unsteady airloads model in FLIGHTLAB[18,19] was used as the baseline reference. The CFD simulation was performed for a range of mean angle of attack α_0, amplitude of oscillations α_c Mach number, and deflection of the control surface δ(t) as shown or a representative simulation, in Table 2. The incremental airloads are then computed as the difference between the CFD based unsteady airloads and the quasi-unsteady baseline. The baseline reference model selected for the implementation does not include any effect of OBC devices. Therefore, the incremental airloads reflect both the effects of OBC and differences between the baseline airloads model and Navier-Stokes based high fidelity CFD simulation. Figure 5 below illustrates the NNET formulation for the ROM that reflects the OBC effects.

The NNET model training is performed with a dedicated module within the FLIGHTLAB.[17] The NNET training makes use of Levenberg-Marquardt algorithm[18] for the training of all three coefficients, i.e., ΔC_{ℓ}, ΔC_{m}, and ΔC_{d}. The selected values of various parameters such as the number of neurons, type of basis function, error tolerance, etc., for the NNET training are shown in Table 3. The number of neurons is selected to be much higher for the drag coefficient as compared to those for the lift and moment coefficients since the drag coefficient data from the CFD analysis shows significantly higher nonlinearity when compared to lift or pitching moment coefficients. The NNET model training is a very time consuming task. By organizing the lift, drag, and pitch moment coefficients into three individual NNET modules, both the NNET model training effort and accuracy were dramatically improved.

Figure 6 shows sample results obtained with the NNET and surrogate models for oscillating airfoils with and without trailing edge flaps.

5. Sample results for Controllers based on Reduced Order Models

The reduced order models of a trailing edge flap developed in the previous section was applied to a testing rotor for evaluation of advanced on-blade control concepts. For illustration, an example on-blade control using active trailing edge flap was evaluated. Figure 7 illustrates the testing example where the trailing edge flap was applied over a blade section from 0.55 to 0.91 of the rotor radius for a generic 4-bladed articulated rotor. The effect of OBC in terms of active trailing edge flap was evaluated. Figure 8 shows the variation of the longitudinal rotor hub force under the excitation of the 2/rev active trailing flap. Compared to the baseline without the active flap excitation, the effect of the on-blade control is apparent in the ROM simulation. Figures 9 and 10 show the variation of the lateral and normal rotor hub force

components, respectively. The application of the active trailing edge flap with the above selected second harmonic profile significantly reduces the oscillatory component of the hub shear force. Notice that the prescribed second harmonic active flap control is an estimated control for functional testing only, instead of an optimized one for overall rotor hub vibratory load reduction. As a result, this profile caused some increase in the hub moment components although it did reduce all the vibratory shear components.

6. LTI MODELS WITH OBC

The two-step methodology[20] for extraction of linear time invariant models of nonlinear systems with time periodic equilibria was evaluated for fidelity of the extracted models. The developed reduced order TEF model combined with a generic helicopter with elastic rotor model in FLIGHTLAB was used for this investigation.

In order to evaluate the fidelity of the extracted LTI models for their use in active rotor power reduction studies, a 2/rev TEF input of 0.5° magnitude and (an arbitrarily selected) 70° phase was used in the LTI model fidelity evaluations. The resulting fixed hub load variations with time as predicted from FLIGHTLAB and from the extracted LTI model are compared in Figure 11a. The LTI model included up to 8/rev harmonic components of rotor MBC states. These included rigid (flap & lag) and elastic modes (first elastic flap and first elastic lag), both. Figure 11b is a zoom-in of results from Figure 11a. The time-domain error index[21] computed using the following equation

$$J^{(1)} = \sqrt{\frac{1}{n_t . n_o} \sum_{i=1}^{n_t} \left[(\Delta y_{data} - \Delta y)_i^T W (\Delta y_{data} - \Delta y)_i \right]}$$

is less than 0.001 indicating good fidelity of the extracted LTI model.

It is well known that N/rev vibration in the fixed system arises from blade force variations in the rotating frame at (N-l)/rev, N/rev and (N+l)/rev vibrations, where N is the number of blades. Hence, it is expected that TEF inputs at these frequencies can be used for vibration control. A TEF input consisting of 3/rev, 4/rev and 5/rev components was used as a way to test the fidelity of the extracted LTI models for their use in active vibration control studies. The magnitudes of the harmonic components of TEF inputs were selected to be 1.0° of 3/rev, 0.5° of 4/rev and 0.25° of 5/rev. The phases of the individual harmonic components were selected arbitrarily. The extracted LTI model included up to 8/rev harmonic components of rotor states. The fixed system hub load responses to the selected TEF input as predicted from FLIGHTLAB is compared with those predicted using the LTI model in Figure 12a with a zoom-in of the results shown in Figure 12b. Even though there is slight deviation in terms of both magnitude and phase visible in the zoom-in plot Figure 12b, the computed time-domain error index of 0.0135 indicates good model fidelity of the extracted LTI model.

In order to verify the LTI model fidelity for its use in active vibration and noise control studies, a test case TEF input with 6/rev and 7/rev components of magnitudes (0.25° of both 6/rev and 7/rev) were used. The predicted fixed system hub load responses from FLIGHTLAB are compared with those from the LTI model predictions in Figure 13a with a zoom-in of the results shown in Figure 13b. Once again, these results demonstrate the fidelity of the extracted LTI models.

7. CONCLUDING REMARKS

A methodology for developing reduced order air loads models of on-blade control concepts based on artificial neural networks (NNET) is described in this study. The developed methodology consists of three steps; creating a CFD database for a selected OBC concept, training of a NNET as an addition to an existing baseline air loads model in order to capture the CFD data base to the required level of fidelity, and integration of the developed NNET of the selected OBC concept into a nonlinear helicopter model. It has been demonstrated that this approach is an effective way of designing onboard controllers.

The developed reduced order models of TEF was integrated with a generic helicopter with elastic rotor model in FLIGHTLAB. Linear time invariant (LTI) models were extracted from the nonlinear helicopter model and the extracted LTI models were evaluated for fidelity for their use in various active rotor control applications using different test cases. It has been shown that the LTI models maintain fidelity for their use in synthesis and design of active rotor controllers using OBC.

8. REFERENCES

[1] Shaw, J., Albion, N., Hanker, E.J. and Teal, R.S, "Higher Harmonic Control: Wind Tunnel Demonstration of Fully Effective Vibratory Hub Force Suppression," AHS 41st Annual Meeting, Texas, May 15-17, 1985.

[2] Jacklin S.A. et al., "Full-Scale Wind Tunnel Test of the McDonnell Douglas Five-Bladed Advanced Bearingless Rotor: Performance, Stability, Loads, Control Power, Vibration and HHC Data," American Helicopter Society Aeromechanics Specialists Conference, San Francisco CA, January 19-21, 1994.

[3] Jacklin, S. A., Blaas, A., Teves, D. and Kube, R., "Reduction of Helicopter BVI Noise, Vibration, and Power Consumption through Individual Blade Control," Proceedings of the 51st Annual Forum of the American Helicopter Society, Fort Worth TX, May 9-11, 1995.

[4] Swanson, S. M., Jacklin, S. A., Blaas, A., Niesl, G. and Kube, R., "Acoustic Results from a Full-Scale Wind Tunnel Test Evaluating Individual Blade Control," Proceedings of the 51st Annual Forum of the American Helicopter Society, Fort Worth TX, May 9-11, 1995.

[5] Norman et al., "Low-Speed Wind Tunnel Investigation of a Full-Scale UH-60 Rotor System," Proceedings of the 58th Annual Forum of the American Helicopter Society, Montreal Canada, June 11-13, 2002.

[6] Jacklin et al., "Full-Scale Wind Tunnel Test of an Individual Blade Control System for a UH-60 Helicopter," Proceedings of the 58th Annual Forum of the American Helicopter Society, Montreal Canada, June 11-13, 2002.

[7] Dawson et al., "Wind Tunnel Test of an Active Flap Rotor: BVI Noise and Vibration Reduction," Proceedings of the 51st Annual Forum of the American Helicopter Society, Fort Worth TX, May 9-11, 1995.

[8] Kottapalli, S. and Straub, F., "Correlation of Smart Active Flap Rotor Loads," Proceedings of the 65th Annual Forum of the American Helicopter Society, Grapevine TX, May 27-29, 2009.

[9] Montanye et al., "Shipboard Helicopter Gust Alleviation Using Active Trailing Edge Flaps," Proceedings of the 65th Annual Forum of the American Helicopter Society, Grapevine TX, May 27-29, 2009.

[10] Arnold, U.T.P., Fürst, D., Neuheuser, T. and Bartels, R., "Development of an Integrated Electrical Swashplate-less Primary and Individual Blade Control System", Cheeseman Award Paper of the 32nd European Rotorcraft Forum, Maastricht, 2006.

[11] Boyd, D.D., "HART-II Acoustic Predictions using a Coupled CFD/CSD Method", Proceedings of the 65th Annual Forum of the American Helicopter Society, Grapevine TX, May 27-29, 2009.

[12] Cheng, R.P., Tischler, M.B. and Celi, R., "A Higher-Order, Time-Invariant, Linearized Model for Application to HHC/AFCS Interaction Study," Proceedings of the 59th Annual Forum of the American Helicopter Society, Phoenix, AZ, May 6-8, 2003.

[13] Pandyan, R. and Sinha, S.C., "Time-Varying Controller Synthesis for Nonlinear Systems subjected to Periodic Parametric Loading," Journal of Vibration and Control, Vol. 7, pp73-90, 2001.

[14] Colaneri, P., Celi, R. and Bittanti, S., "Constant Coefficient Representations of Discrete Periodic Linear Systems," Proceedings of the 4th Decennial Specialists' Conference on Aeromechanics, San Francisco, CA, Jan 21-24, 2004.

[15] Chandrasekhara, M. S. and Carr, L. W., "Unsteady stall Control using Dynamically Deforming Airfoils," AIAA Journal, Vol. 36, No. 10, 1998.

[16] Sahin, M.., Sankar L. N., Chandrasekhara, M. S., Tung, C. "Stall alleviation Using a Deformable Leading Edge Concept," AIAA 2000-0520, 38th AIAA Aerospace Sciences Meeting, Reno, NV 2000.

[17] Haykin, Simon, Neural Networks, 2nd edition, Prentice Hall, 1999.

[18] FLIGHTLAB X-Analysis User Manual, Advanced Rotorcraft Technology, Inc., 2008.

[19] FLIGHTLAB Theory Manuals 1 & 2, Advanced Rotorcraft Technology, Inc., 2008.

[20] Prasad, J. V. R., Olcer, F. E., Sankar, L. N. and He, C., "Linear Time Invariant Models for Integrated Flight and Rotor Control," Proceedings of the 35th European Rotorcraft Forum, Hamburg, Germany, September 22 – 25, 2009.

[21] Tischler, M.B. and Remple, R.K.: Aircraft and Rotorcraft system Identification: Engineering Methods with Flight Test Examples, AIAA Publications, Virginia, USA, 2006.

Table 1. Effect of VDLE VR-12 Airfoil on Critical Quantities

	Experiment	Computed
Peak C_L Reduction	8%	5%
Peak C_D Reduction	63%	57%
Peak C_M Reduction	31%	49%

Table 2. Parameters for a Representative CFD run

Mach Number	Airfoil AoA	OBC Angle
M=[0.3 0.4]	α_o=[15 10 5 0 -6]	δ_c=[7 4 0]
	α_c=[10 5 2.5]	φ_δ=[0 90 180]
	k=[0 0.03 0.05 0.10]	k_δ=[0.5 1.0]k
M=[0.5 0.6]	α_o=[7 3 0 -3]	δ_c=[5 3 0]
	α_c=[4 2]	φ_δ=[0 90 180]
	k=[0 0.03 0.05 0.10]	k_δ=[0.5 1.0]k
M=[0.7]	α_o=[5 2 0 -2]	δ_c=[3 1.5 0]
	α_c=[2 1]	φ_δ=[0 90 180]
	k=[0 0.03 0.05 0.10]	k_δ=[0.5 1.0]k

Mach Number	Airfoil AoA	OBC Angle
M=[0.3 0.4]	α_o=[15 10 5 0 -6]	δ_c=[7 4 0]
	α_c=[10 5 2.5]	φ_δ=[0 90 180]
	k=[0 0.03 0.05 0.10]	k_δ=[0.5 1.0]k
M=[0.5 0.6]	α_o=[7 3 0 -3]	δ_c=[5 3 0]
	α_c=[4 2]	φ_δ=[0 90 180]
	k=[0 0.03 0.05 0.10]	k_δ=[0.5 1.0]k
M=[0.7]	α_o=[5 2 0 -2]	δ_c=[3 1.5 0]
	α_c=[2 1]	φ_δ=[0 90 180]
	k=[0 0.03 0.05 0.10]	k_δ=[0.5 1.0]k

Table 3. Parameters for NNET training

	ΔC_d	ΔC_l	ΔC_m
Hidden Neurons	34	17	17
Hidden Activation Function	Tangent Hyperbolic	Tangent Hyperbolic	Tangent Hyperbolic
Output Activation Function	Linear (-∞,+∞)	Linear (-∞,+∞)	Linear (-∞,+∞)
Error Tolerance	10^{-6}	10^{-6}	10^{-6}
Maximum iterations	10	10	10

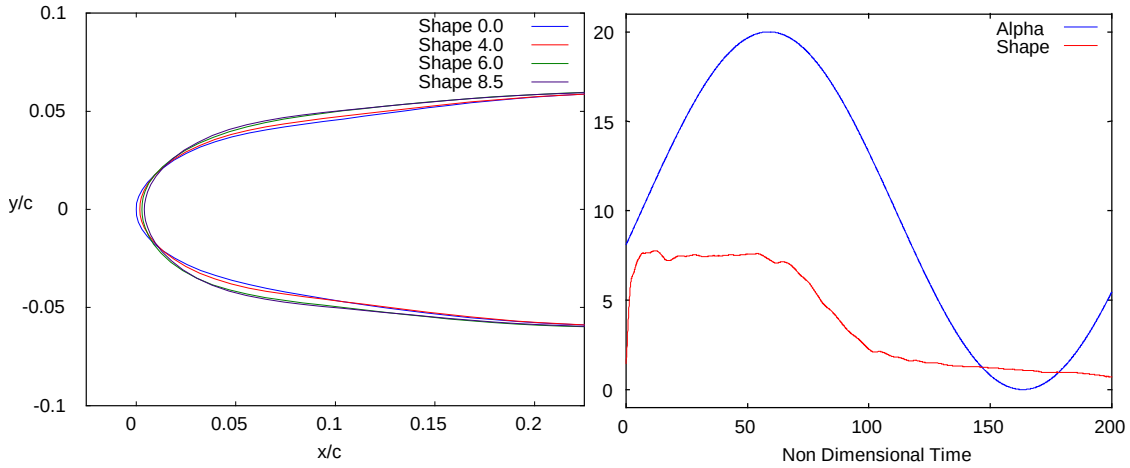

Figure 1. Variation of Leading Edge Shape with Angle of Attack

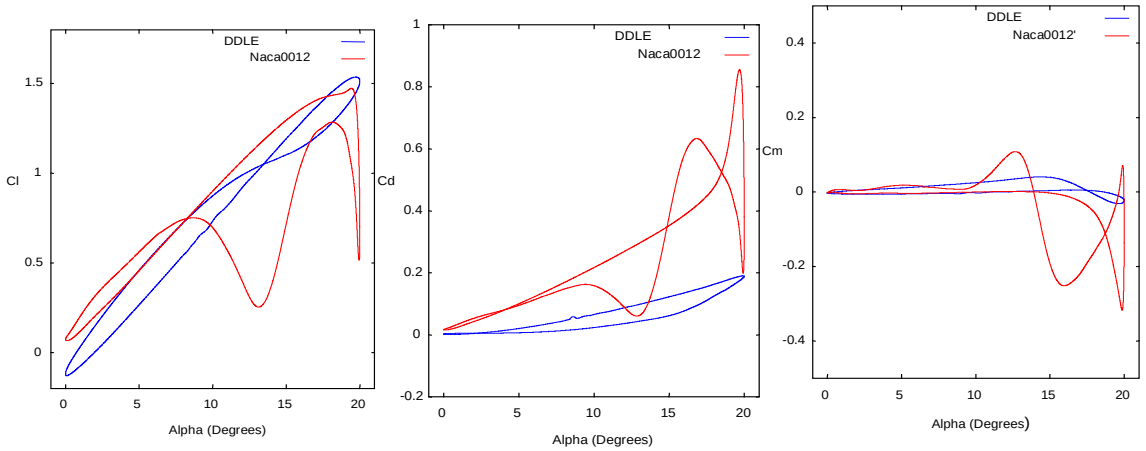

Figure 2. Comparison of computed Lift, Moment and Drag Hysteresis Loops between the NACA 0012 and the DDLE Airfoils

C-type Grids for NACA0012 & VR-7

C-type Grids for NACA0012 &VR-7 with 15 deg Droop

Figure 3. Body-Fitted Grids for NACA 0012 and VR-7 Airfoils with a Drooped leading Edge

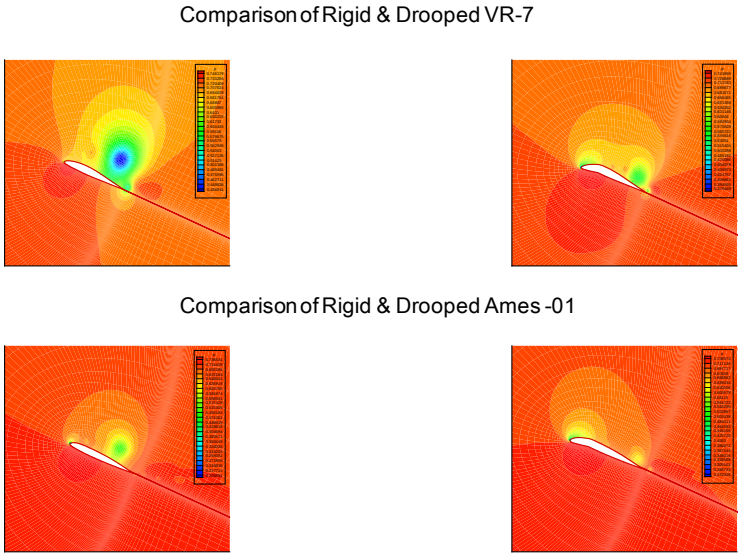

Figure 4. Pressure Field over VR-7 and Ames-01 airfoils with and without Droop at 24.7° Upstroke

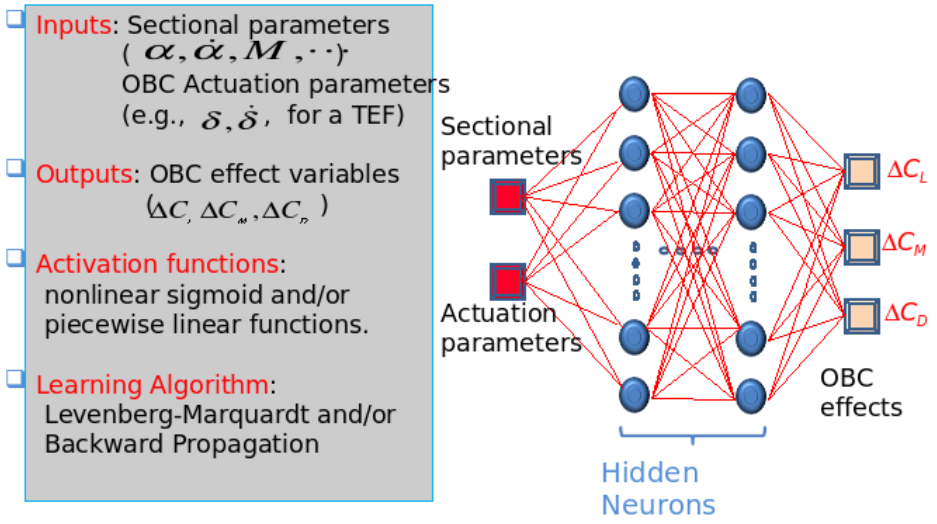

Figure 5. Reduced Order Model based on Neural Network

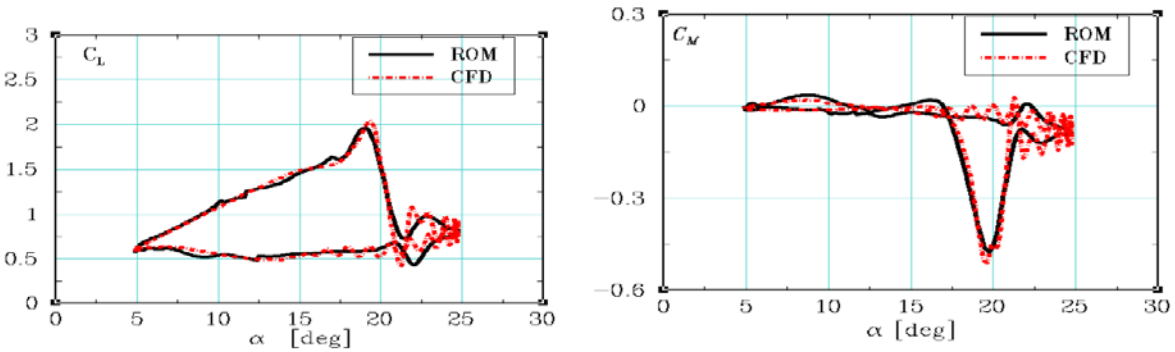

Figure 6a. Computed and Predicted Lift Hysteresis Loops for a SC 1095 Airfoil in Deep Stall

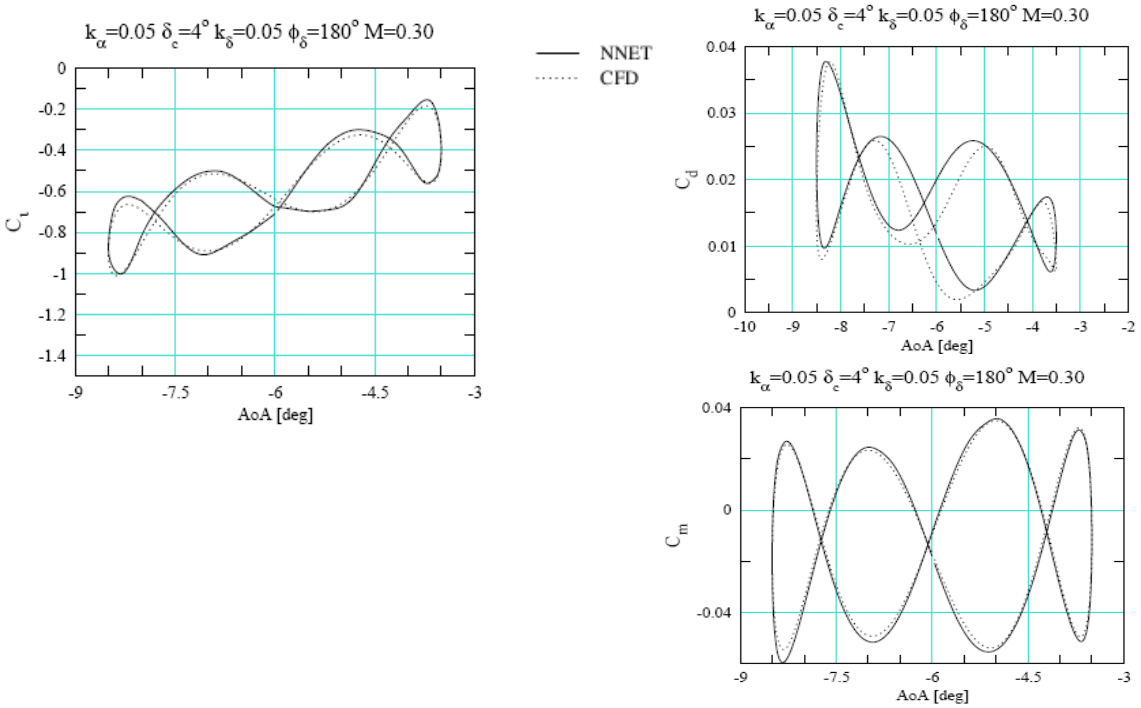

Figure 6b. Computed and Predicted Moment Hysteresis Loops for a SC 1095 Airfoil +Flap

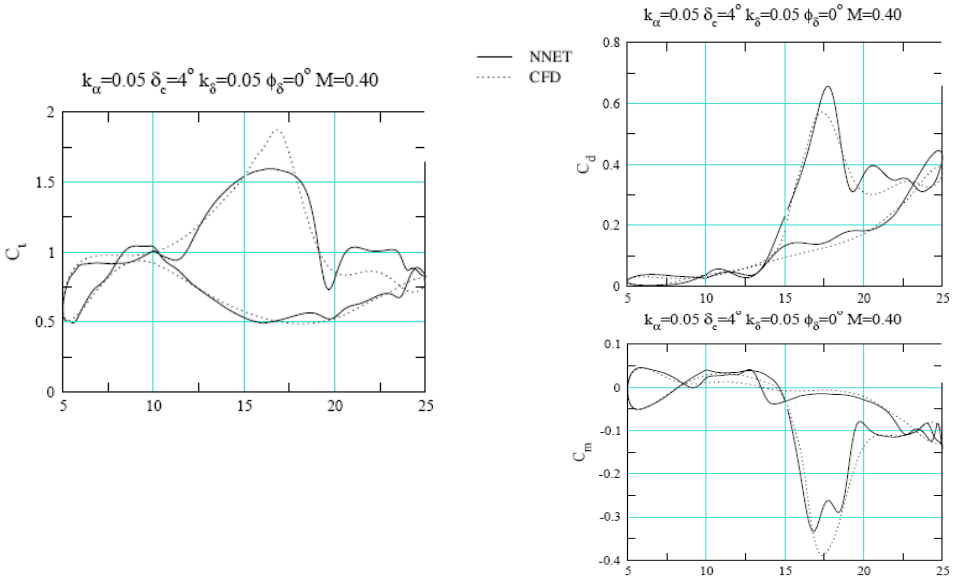

Figure 6c. Computed and Predicted Moment Hysteresis Loops for a SC 1095 Airfoil +Flap

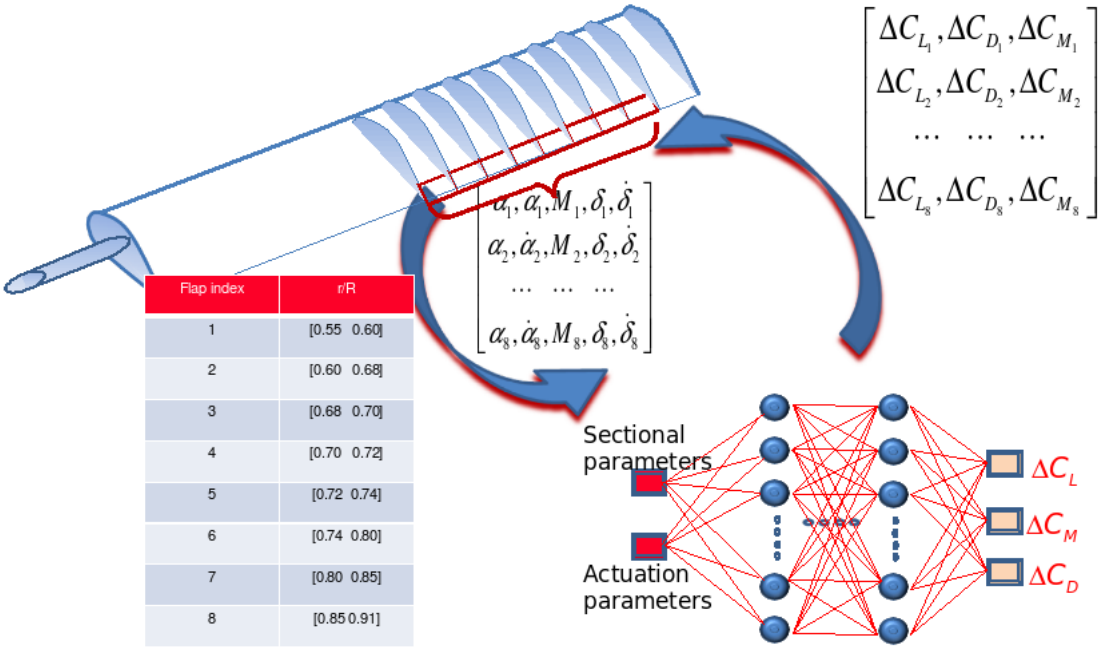

Figure 7. Implementation of ROM for active trailing flap control studies

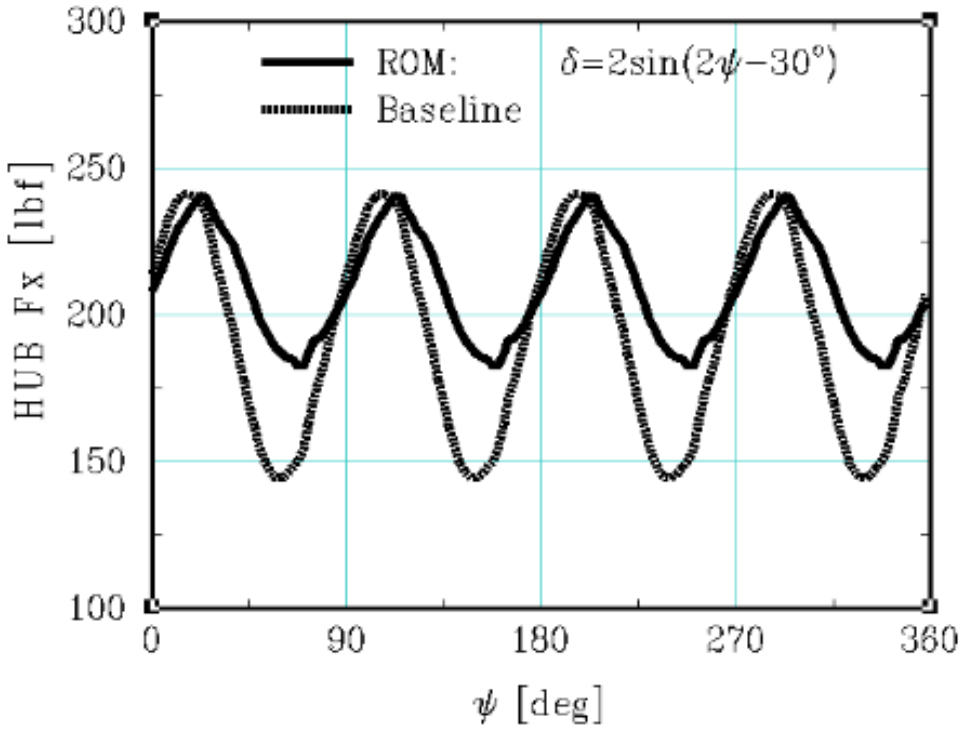

Figure 8. Effect of active trailing flap on rotor hub force (F_x)

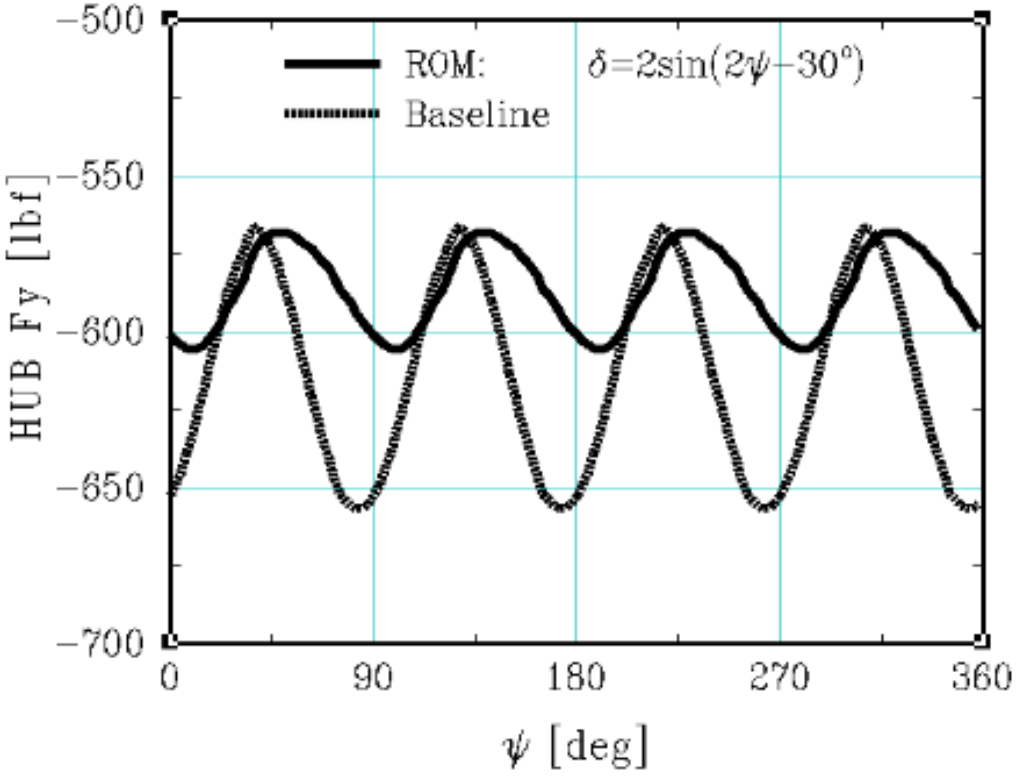

Figure 9. Effect of active trailing flap on rotor hub force (F_y)

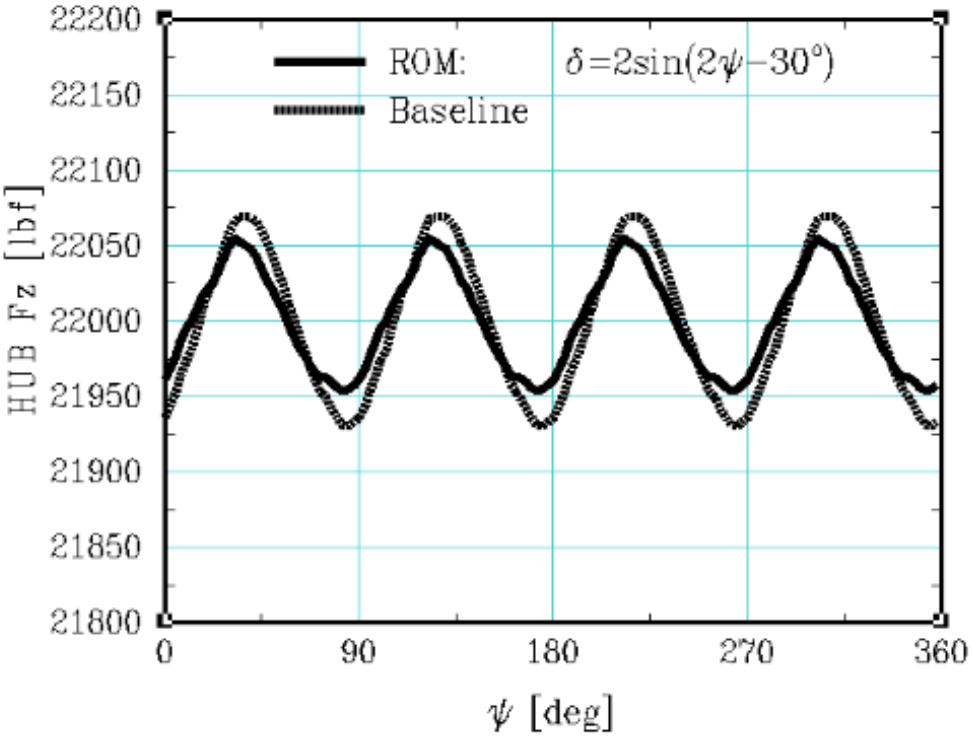

Figure 10. Effect of active trailing flap on rotor hub force (F_z)

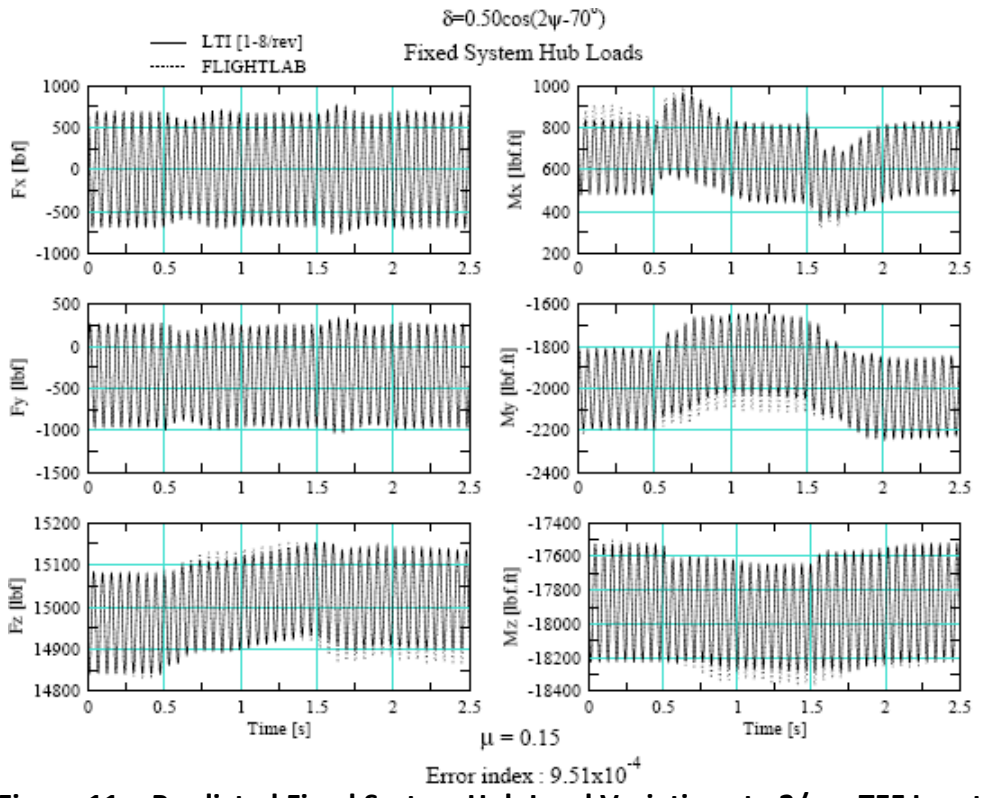

Figure 11a. Predicted Fixed System Hub Load Variations to 2/rev TEF Input.

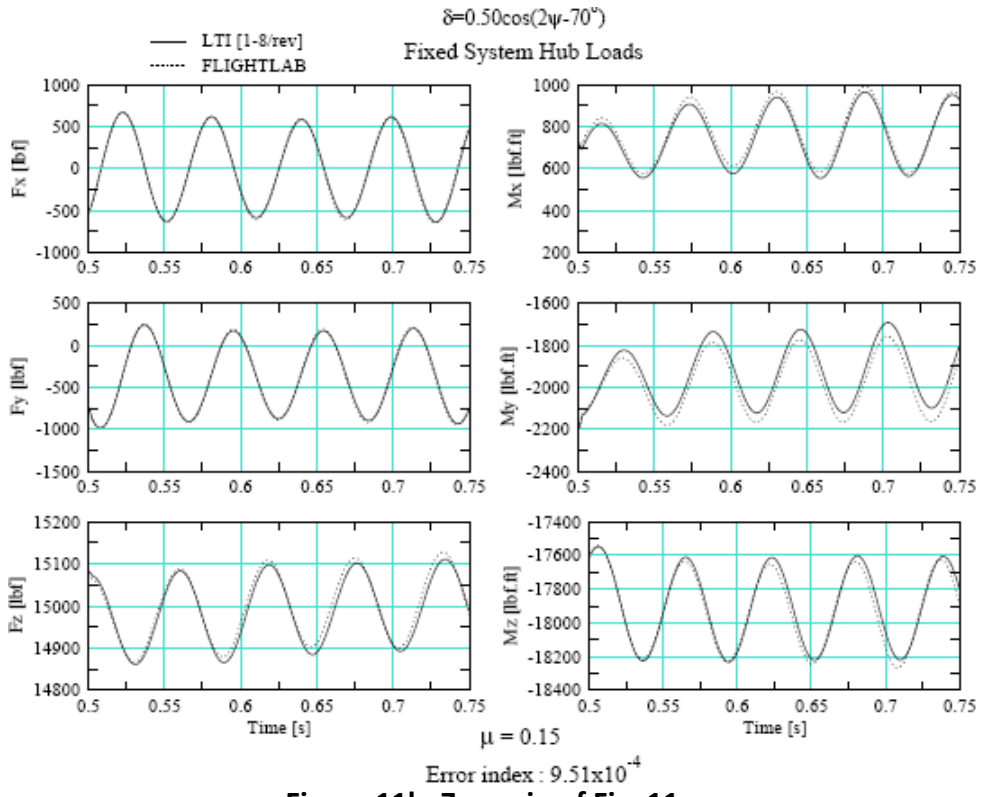

Figure 11b. Zoom-in of Fig. 11a.

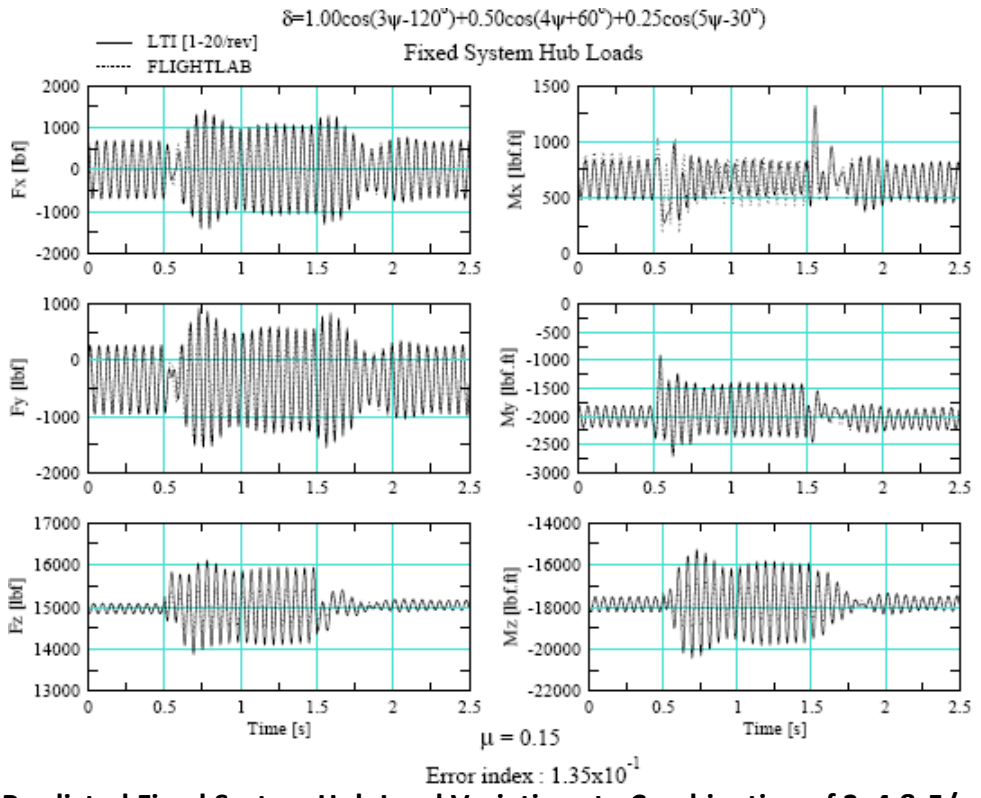

Figure 12a. Predicted Fixed System Hub Load Variations to Combination of 3, 4 & 5/rev TEF Input.

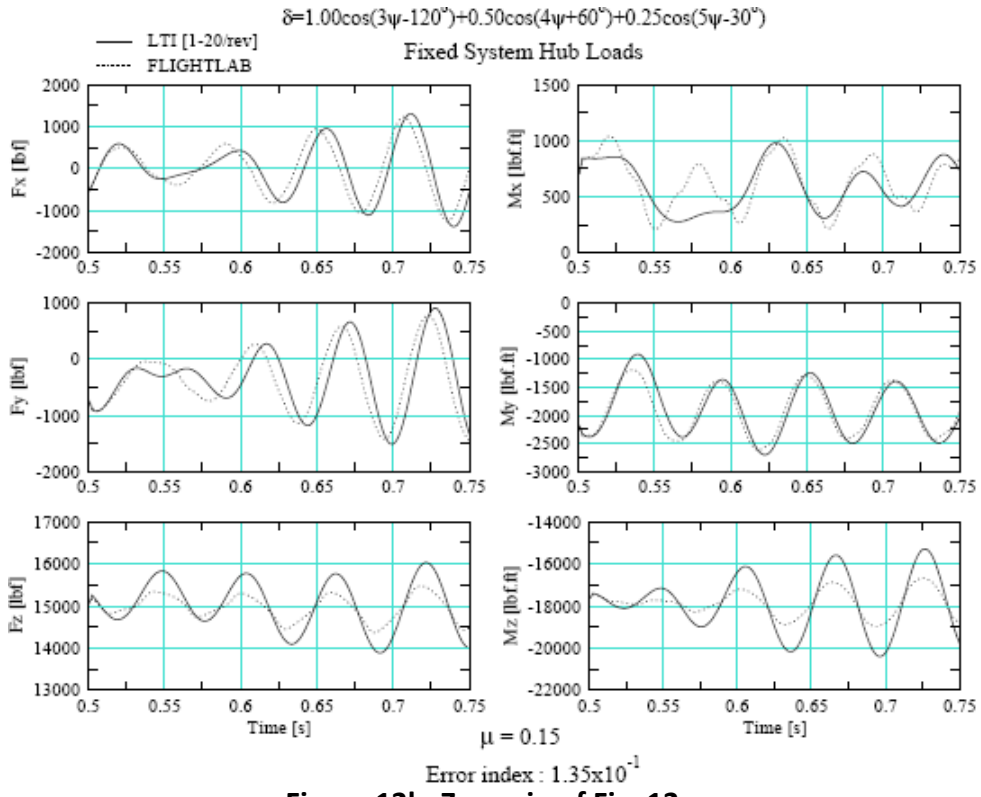

Figure 12b. Zoom-in of Fig. 12a.

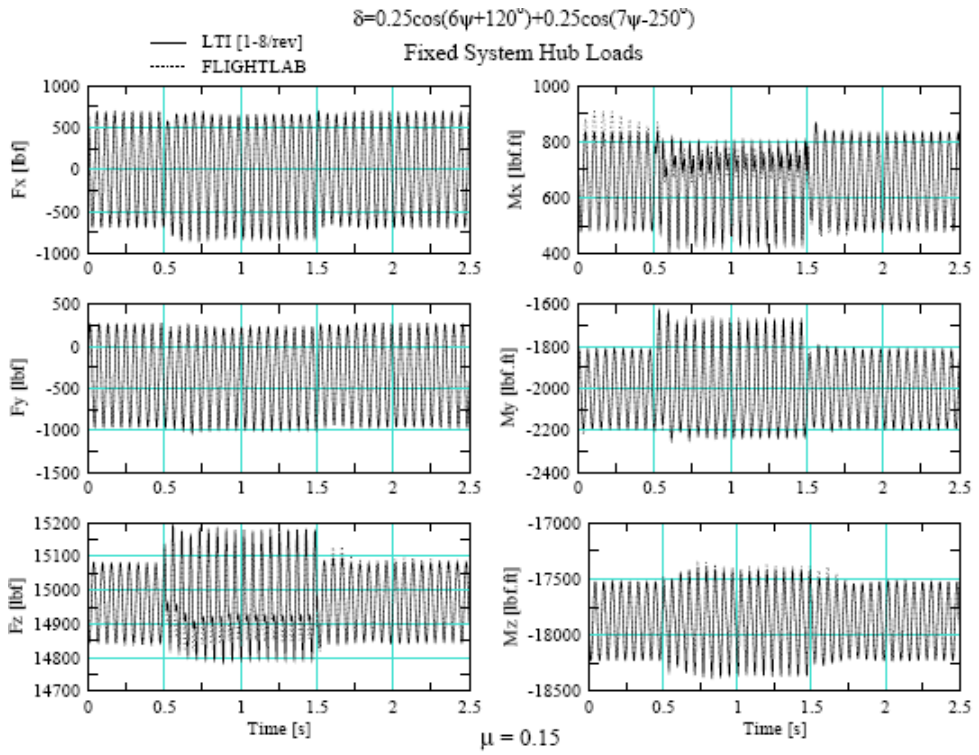

Figure 13a. Predicted Fixed System Hub Load Variations to Combination of 6 & 7/rev TEF Input (1-8/rev).

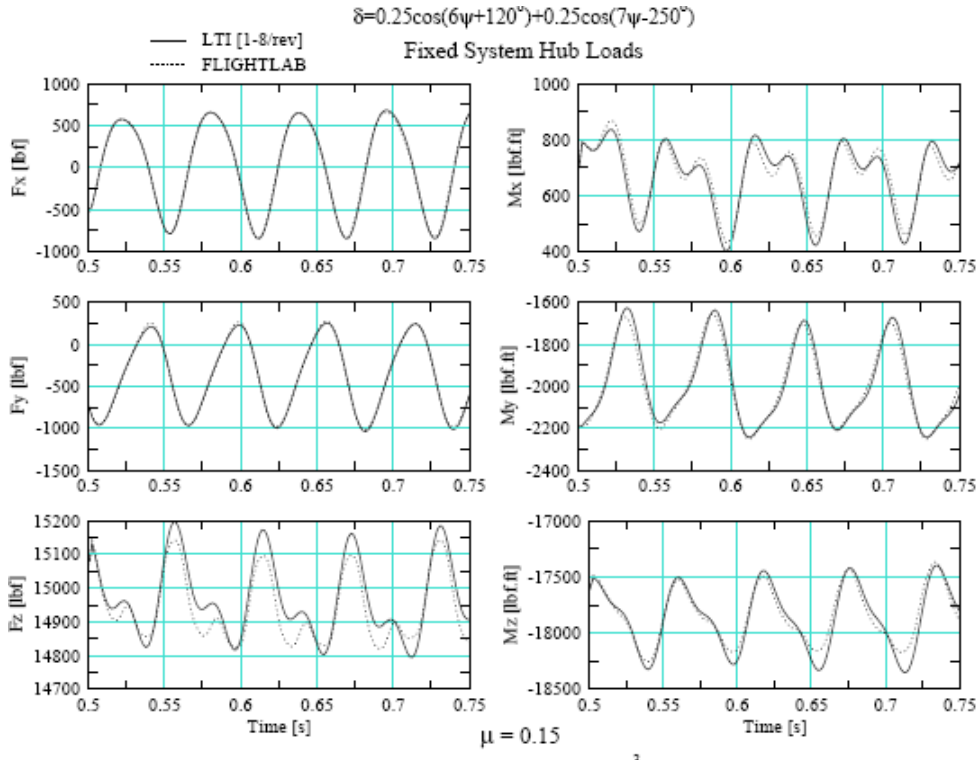

Figure 13b. Zoom-in of Fig. 13a.